Shock-Induced Dynamic Stall

L E Ericsson* and J P Reding†
Lockheed Missiles & Space Company, Inc , Sunnyvale, California

At freestream Mach numbers above $M=0\,3$ shock/boundary layer interaction begins to complicate the unsteady airfoil stall characteristics The present paper shows how theoretical relationships can be developed for the interdependence between unsteady and steady characteristics to provide the means whereby the shock induced dynamic stall characteristics can be determined if the static characteristics are known, e g , from ex periments

Nomenclature

a = total time lag parameter Eq (15)
c = two dimensional chord length
d = sectional drag; coefficient $c_d = d/(\rho_\infty U_\infty^2/2)c$
f = frequency
h = cross sectional thickness
k_M = shock movement parameter Eq (11)
l = sectional lift; coefficient $c_l = 1/(\rho_\infty U_\infty^2/2)c$
M = Mach number
m_p = sectional pitching moment; coefficient $c_m = m_p/(\rho_\infty U_\infty^2/2)c^2$
n = sectional normal force; coefficient $c_n = n/(\rho_\infty U_\infty^2/2)c$
q = pitch rate
r = radius
t = time
U = velocity
$\bar{U}$ = convection velocity
x = chordwise distance from leading edge
α = angle of attack
α_0 = trim angle of attack
Δ = increment and amplitude
Δh = height above ground plane
θ = perturbation in pitch
ξ = dimensionless x coordinate $= x/c$
ξ_c = convective time lag parameter
ξ_{sh} = effect of shock movement
ξ_{sp} = effect of separation point movement
ξ_w = Kármán Sears wake lag parameter
ρ = air density
ρ_N = dimensionless nose radius $= r/c$
τ = dimensionless time $= U_\infty t/c$
$\omega\ \bar{\omega}$ = angular frequency; $\omega = 2\pi f\ \bar{\omega} = \omega c/U_\infty$

Subscripts

a = atttached flow
c = critical
OC = oscillation center or rotation axis
d = discontinuity
h = hysteresis
LP = local peak
N = nose
s = separated flow
sh = shock
sp = separation point
TH = theoretical
v = vortex
w = wake
∞ = freestream conditions

Derivatives

$c_{m\alpha} = \partial c_m/\partial\alpha$
$\dot{\alpha} = \partial\alpha/\partial t$
$c_{m_{\dot{\theta}}} = \partial c_m/\partial(c\dot{\theta}/U_\infty)$‡
$c_{\bar{m}_{\dot{\theta}}}$ = integrated mean value the "effective damping derivative"

Introduction

INCOMPRESSIBLE (low speed) dynamic stall has received a great deal of attention[1,2] and methods have been developed for prediction of the associated unsteady aerodynamics [3,4] However it is only recently that serious attempts have been made to investigate what role the shock/boundary layer interaction plays in the dynamic stall phenomenon McCroskey et al [5,6] found that the peak velocity on a stalling airfoil exceeded sonic speed already when $M_\infty > 0\,2$ (Fig 1) The analytic method developed in Ref 7 for prediction of the peak velocity ratio at low subsonic Mach numbers, when $U_{LP}/U_\infty \approx M_{LP}/M_\infty$ can predict M_{LP} through the transonic range with less than 10% error The same analysis showed that $M_\infty > 0\,35$ would be required for the appearance of a strong terminal shock This is in basic agreement with the experimental results in Ref 5 where no shocks were observed in the tested Mach number range $M \leq 0\,3$, but the authors expressed the expectation that such shocks would appear if the Mach number was increased beyond $M = 0\,3$

These results indicate that shock/boundary layer in teraction will enter into the dynamic stall picture in many flow conditions of practical interest The present paper shows how theoretical relationships can be developed for prediction of the shock induced dynamic stall characteristics using ex perimental static characteristics

Analysis

The dynamic stall characteristics are determined by superimposing the effects of separated flow upon the attached flow unsteady aerodynamics determined by use of thin airfoil theory [8,9]

Linear Analysis Results

For small oscillation amplitudes and low frequencies $|\dot{\theta}c/U| \ll 1$ and $\bar{\omega}^2 \ll 1$ the local linearization concept can be applied even to the nonlinear separated flow aerodynamics as long as the characteristics are continuous in nature This

Received March 16 1983; revision received Aug 25 1983

*Senior Consulting Engineer Fellow AIAA
†Staff Engineer Associate Fellow AIAA

‡In Refs 16 and 17 the half chord $c/2$ rather than c is used as a reference giving twice the magnitude of the damping derivatives compared to those herein

permits the dynamic stall characteristics to be determined by very simple analytic means.

The attached flow damping, $c_{m\dot{\theta}_a}$, is obtained as follows[8,9]

$$c_{m\dot{\theta}_a} = c_{n\alpha}[\xi_w(0.25-\xi_{OC})+0.25(\xi_{OC}-0.75)] \quad (1)$$

where ξ_w is the Karman-Sears wake-lag parameter,[10] giving the phase lag $\omega\Delta t_w = \omega\xi_w$. ξ_w can be approximated as follows[8]:

$$\xi_w = 1.5, \qquad \omega \le 0.16$$
$$= 0.245/\omega, \qquad \omega > 0.16 \quad (2)$$

Experimental results[11] indicate that the attached flow normal force slope, $c_{n\alpha} = c_{l\alpha} + c_d$, can be approximated by the thin airfoil lift slope, $c_{l\alpha} = 2\pi$, even for thick rectangular cross sections. Compressibility effects are accounted for using the Prandtl-Glauert compressibility correction up to $M_\infty = 0.9$, where the agreement with experiment ceases.[9] Thus, one obtains

$$(c_{n\alpha})_{TH} = 2\pi/\sqrt{1-M^2} \qquad M < 0.9 \quad (3)$$

The static derivative $c_{m\alpha_a}$ in static tests, and $c_{m\dot{\theta}_a}$ in dynamic tests, is obtained simply as

$$c_{m\dot{\theta}_a} = -(c_{n\alpha})_{TH}(0.25-\xi_{OC}) \quad (4)$$

The difference between $c_{m\dot{\theta}a}$ and experimental results is the effect of flow separation on static stability

$$\Delta c_{m\dot{\theta}_s} = c_{m\alpha} - c_{m\dot{\theta}_a} \quad (5)$$

It has been described previously how the corresponding separation-induced dynamic effect can be defined by the use of an effective time lag. In the case of a flare-cylinder body[12] (Fig. 2) the separated shear layer impacting on the flare at time t, when $\alpha(t) = 0$, was generated by the nose at a time increment Δt earlier, when the angle of attack was $\alpha(t-\Delta t) > 0$. Thus, a residual flare force exists at $\alpha(t) = 0$, which drives the motion. Consequently due to the time lag the statically stabilizing flare force has a dynamically destabilizing effect.

In the case of a pitching airfoil[8] the situation is very similar. The aerodynamic loading existing at $\alpha(t) = 0$ is the residual effect of flow conditions initiated a time increment earlier, when $\alpha(t-\Delta t) > 0$. Also the time history effect in this case can be described by the use of a lumped, finite time lag, as has been demonstrated.[8] One then obtains the following expression for the separation-induced dynamic effect.

$$\Delta c_{m\dot{\theta}_s} = -\Delta\tau_s \Delta c_{m\dot{\theta}_s} \quad (6)$$

where $\Delta c_{m\dot{\theta}_s}$ is given by Eq. (5) and $\Delta\tau_s$ is the effective time-lag parameter

$$\Delta\tau_s = \xi_w + \xi_c + \xi_{sp} + \xi_{sh} \quad (7)$$

It is shown in Ref. 4 that in the case of dynamic stall the Karman-Sears wake-lag parameter ξ_w is no longer frequency

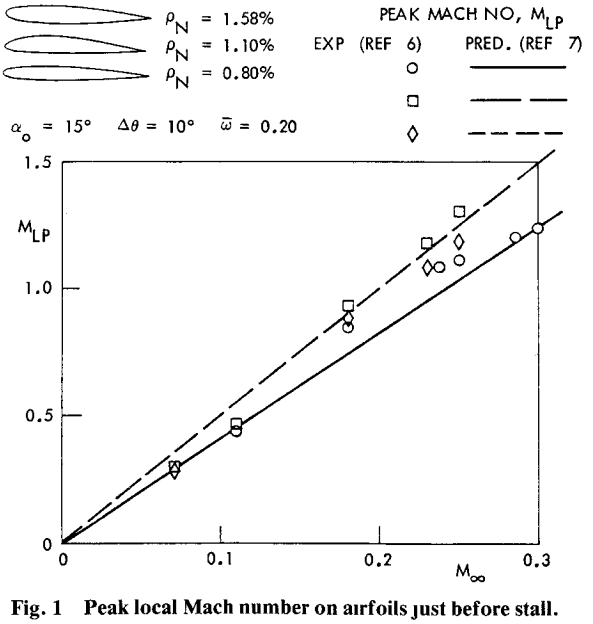

Fig. 1 Peak local Mach number on airfoils just before stall.

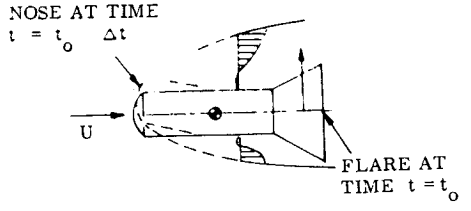

Fig. 2 Effect of time lag.

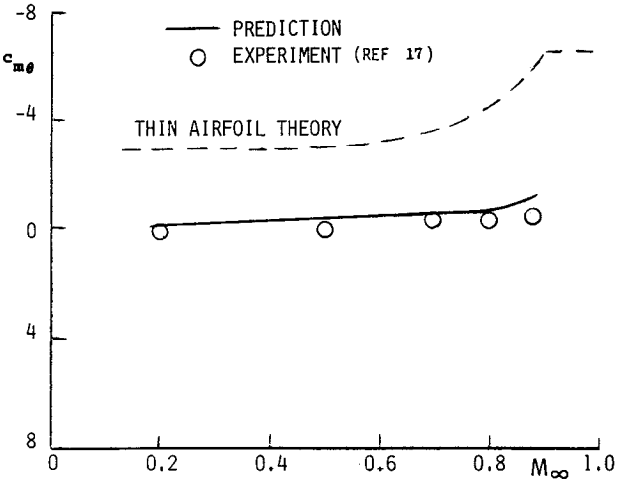

a) Sharp-edged corner.

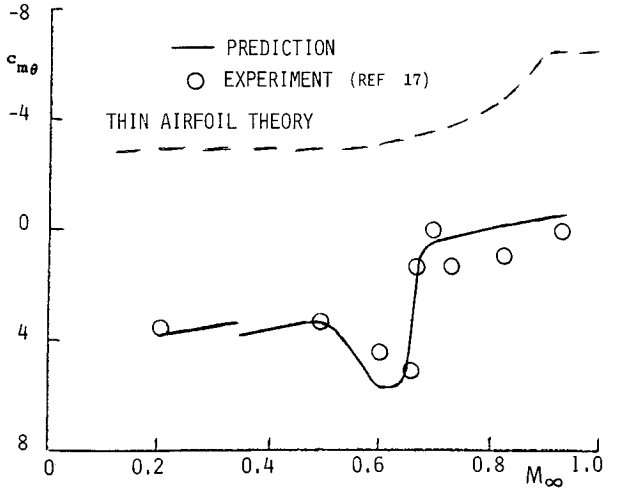

b) Corner radius, $r/h = 0.13$.

Fig. 3 Damping characteristics of a $c/h = 2$ rectangular cross section as determined by experiment and linear analysis.

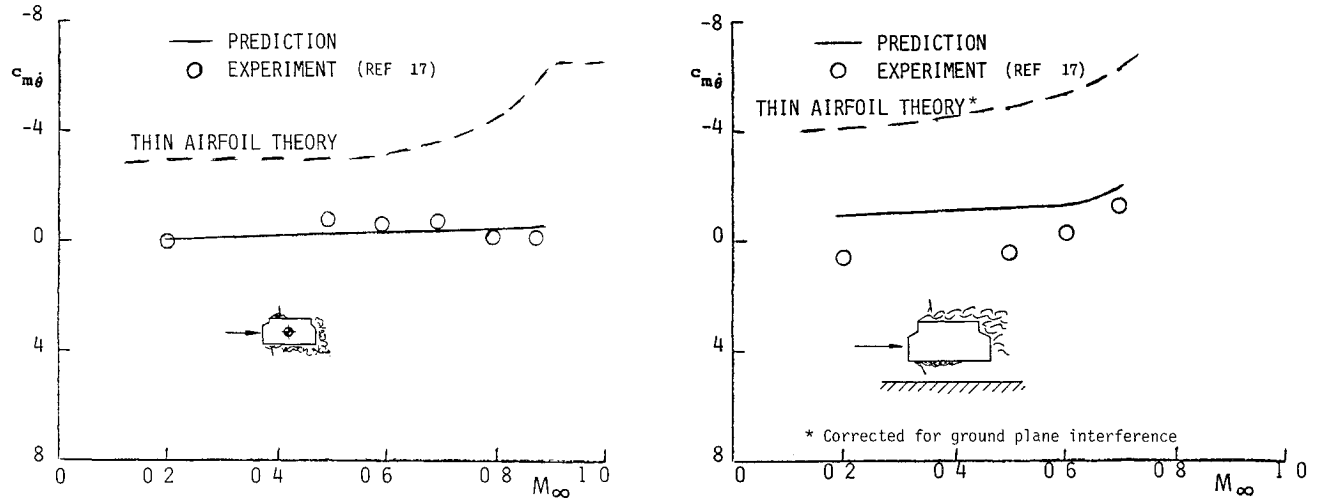

a) Without groundplane $\Delta h/h = \infty$ b) With groundplane $\Delta h/h = 0\ 55$

Fig 4 Damping characteristics of an indented $c/h = 2$ rectangular cross section as determined by experiment and linear analysis

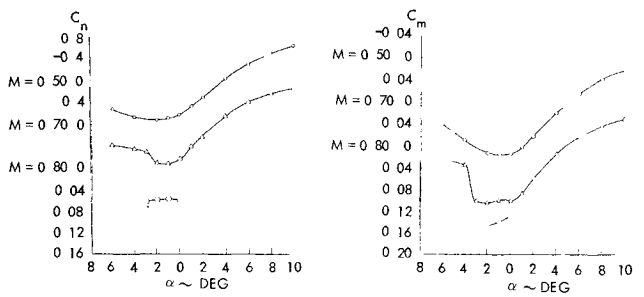

Fig 5 Static aerodynamic characteristics of an indented $c/h = 2$ rectangular cross section at $\Delta h/h = 0\ 55$ (Ref 21)

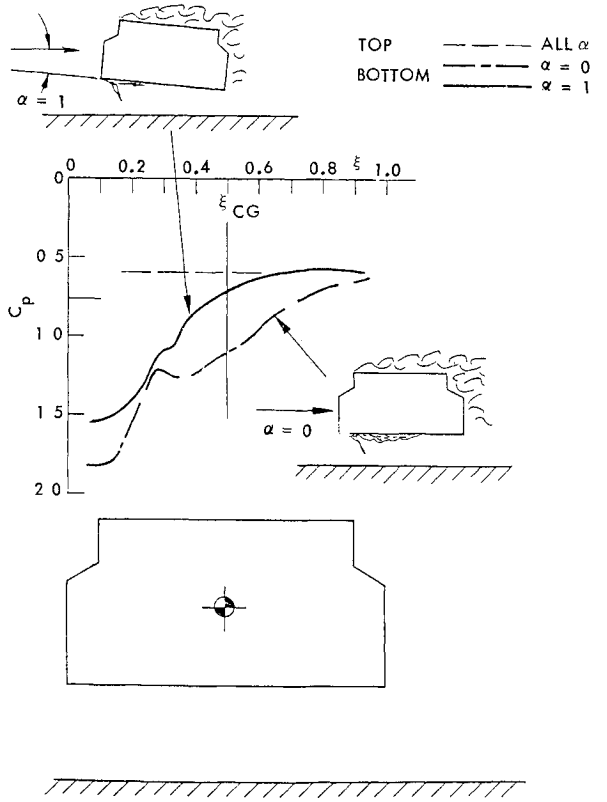

Fig 6 Static pressure distribution on an indented $c/h = 2$ rectangular cross section at $\Delta h/h = 0\ 55$ and $M_\infty = 0\ 7$ (Ref 21)

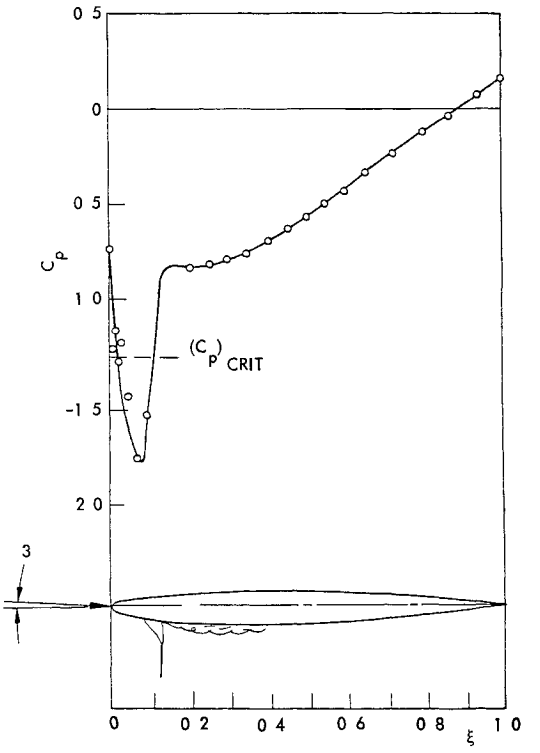

Fig 7 Static pressure distribution on a high performance airfoil at $M_\infty = 0\ 6$ (Ref 21)

limited as in the attached flow case [8 10] Eq (2) but remains constant

$$\xi_w = 1\ 5 \tag{8}$$

For separation well downstream of the leading edge there is in addition to ξ_w a delay ξ_c of separation due to the time required to convect upstream pressure gradient effects down through the boundary layer to the separation point ξ_s This can be expressed as follows:

$$\xi_c = \xi_s U_\infty / \bar{U} \tag{9}$$

where $\bar{U}$ is the mean convection velocity

The time lag due to the effect of the moving separation point ξ_{sp} takes the value $\xi_{sp} \approx 0\ 75$ for turbulent boundary

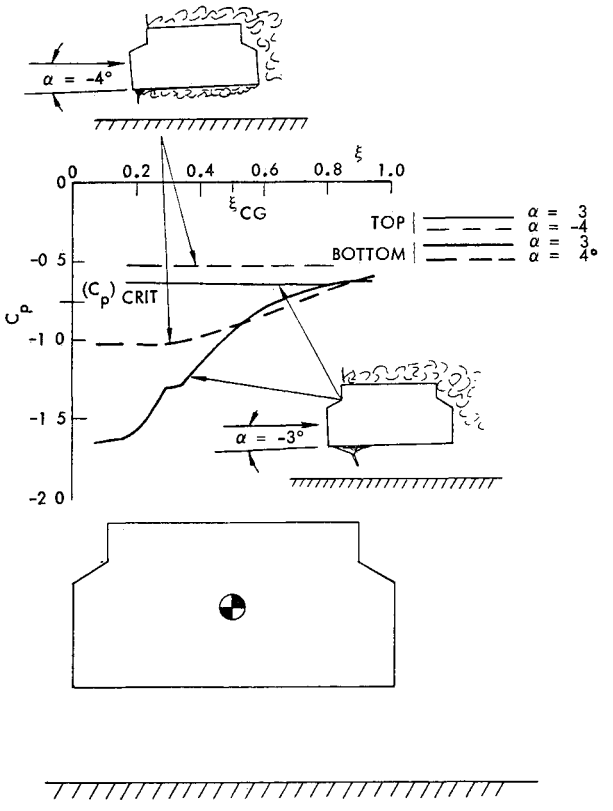

Fig 8 Static pressure distributions showing the effect of sudden flow separation on an indented $c/h=2$ rectangular cross section at $\Delta h/h=0\ 55$ and $M_\infty=0\ 7$ (Ref 21)

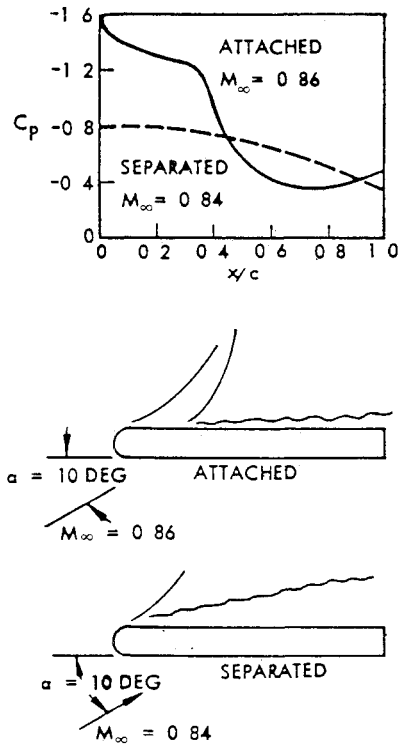

Fig 9 Sudden separation effects on a slab wing airfoil section (Ref 23)

layer separation which is the prevalent dynamic stall type [13] Thus

$$\xi_{sp}=0 \quad \text{Separation fixed}$$

$$=0\ 75 \quad \text{Separation free to move} \qquad (10)$$

In addition to the above time lag parameters valid for incompressible flow one has to add the effective time lag parameter ξ_{sh} for $M_\infty>0\ 35$ to account for the effect of a moving terminal shock According to the analysis in Ref 14 one can define ξ_{sh} as follows:

$$\xi_{sh}=0 \quad M_\infty<0\ 35 \quad M_\infty \geq M_c$$

$$=k_M M \quad 0\ 35< M_\infty<M_c \qquad (11)$$

For the airfoil tested by Lambourne [15] one obtains[14] $k_M \approx 1\ 2$ which for lack of other data is the value used in the present analysis M_c is the Mach number at which the shock with associated flow separation has become fixed at the leading edge

The analytic means described above were used recently in the analysis of the aeroelastic stability of the Space Shuttle cable trays [16] Initially the exterior of the cable tray consisted of a rectangular cross section with a chord to height ratio of 2 $c/h=2$ Because of the unknown structural characteristics of the heatshield material used the corner was assumed to vary from being completely sharp to having a corner radius of $r/h=0\ 13$ In both cases flow separation starts at the leading edge and $\xi_c=0$ For the sharp corner the flow separation is fixed i e $\xi_{sp}=\xi_{sh}=0$ For the rounded corner $M_c=0\ 66$ according to the experimental data trend [17] Thus $\xi_w=1\ 5$ $\xi_{sp}=0\ 75$ and ξ_{sh} is given by Eq (11) The oscillation center was at $\xi_{OC}=0\ 5$ in all cases Figure 3 shows that the predicted pitch damping is in rather good agreement with the ex perimental results [17 18]

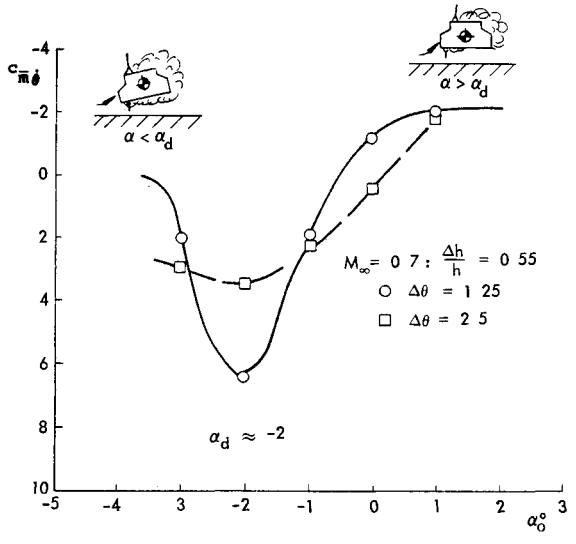

Fig 10 Effect of angle of attack and oscillation amplitude on measured damping (Ref 17)

The prediction for the indented cross section representing a later design of the Space Shuttle cable tray [19] is also in good agreement with experiment[17 18] (Fig 4a) In the presence of a ground plane the attached flow damping the thin airfoil theory curve in Fig 4b had to be corrected for ground in terference effects [19 20] The reason for the deviation between pediction and experiment in this case (Fig 4b) is probably the effect of the ground plane It causes complete leeside flow separation and the thin airfoil value $\xi_w=1\ 5$ which assumes that the shed vorticity is convected downstream with freestream velocty should probably be modified by the mean separated flow velocity [11] i e

$$\xi_w=1\ 5U_\infty/\bar{U} \qquad (12)$$

where $\bar{U}/U_\infty<1\ 0$

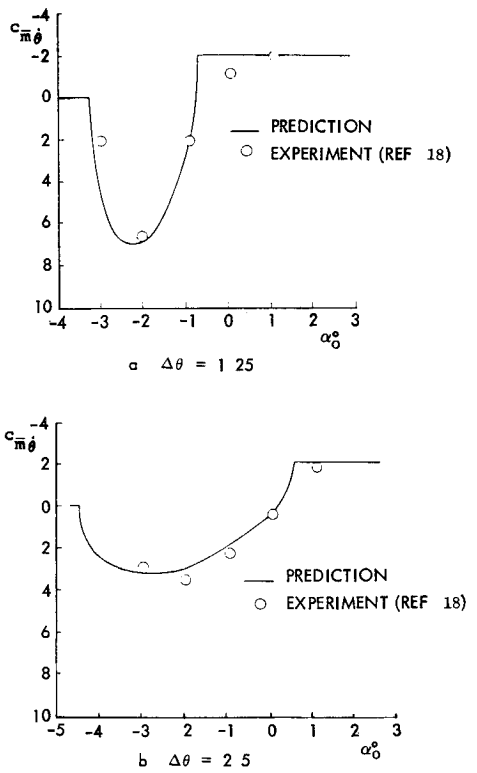

Fig 11 Comparison between predicted and measured nonlinear damping characteristics at $M_\infty = 0\ 7$

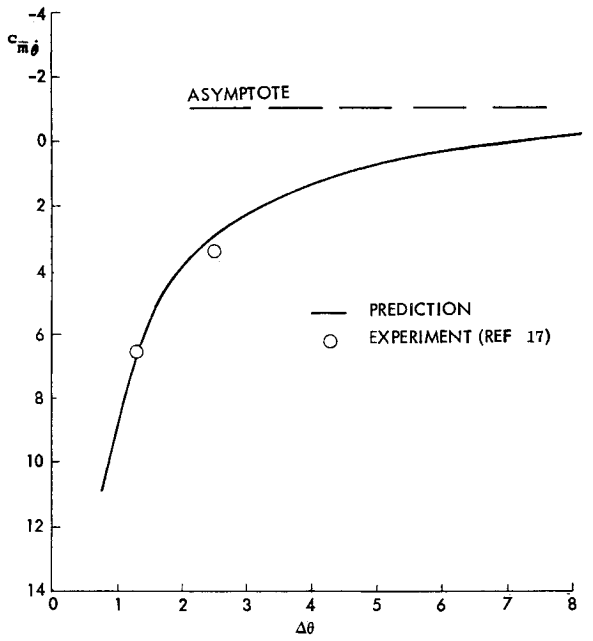

Fig 12 Comparison between predicted and measured adverse damping characteristics

It should be emphasized that the agreement between prediction and experiment in Figs 3 and 4 is unexpectedly good, considering that the analytic method was developed for airfoils and not for the bluff cross sections to which it has been applied in Figs 3 and 4

The static experimental results[21] indicate that the aerodynamic characteristics are continuous at $\alpha = 0$ (Fig 5) and that the bottom side pressure distribution on the indented rectangular cross section (Fig 6) is similar to the leeside pressure distribution measured on a high performance air foil[22] (Fig 7) However at $M_\infty = 0\ 7$, a discontinuous change of the aerodynamic characteristics takes place at $\alpha_d \approx -3$ deg (Fig 8) The pressure distribution shows that complete flow separation on the bottom side occurs when α is changed from $\alpha = -3$ to -4 deg Again, the results are rather similar to the sudden separation effects observed on the top side of an airfoil[23] (Fig 9) In order to consider the effect of the sudden separation on the dynamic characteristics a nonlinear analysis is required

Nonlinear Analysis Results

The nonlinear damping analysis of Refs 12 and 24 gives the following "effective damping derivative" i e the linear measure of the energy dissipation per oscillation cycle in dynamic tests where $\bar{\omega}^2 \ll 1$

$$c_{m\dot{\theta}} = c_{m\dot{\theta}_2} - \frac{1}{\pi}\frac{\Delta c_{m_d}}{\Delta\theta}\left\{a\left[\sqrt{1-\left(\frac{\alpha_0+\alpha_d+\Delta\alpha_h}{\Delta\theta}\right)^2} + \sqrt{1-\left(\frac{\alpha_0-\alpha_d-\Delta\alpha_h}{\Delta\theta}\right)^2} + \sqrt{1-\left(\frac{\alpha_0+\alpha_d}{\Delta\theta}\right)^2} + \sqrt{1-\left(\frac{\alpha_0-\alpha_d}{\Delta\theta}\right)^2}\right] + \frac{2}{(\omega c/U)}\frac{\Delta\alpha_h}{\Delta\theta}\right\} + \frac{c_{m\dot{\theta}_1} - c_{m\dot{\theta}_2}}{2\pi}$$

$$\times\left[\arcsin\frac{\alpha_0+\alpha_d+\Delta\alpha_h}{\Delta\theta} - \arcsin\frac{\alpha_0-\alpha_d-\Delta\alpha_h}{\Delta\theta} + \arcsin\frac{\alpha_0+\alpha_d}{\Delta\theta} - \arcsin\frac{\alpha_0-\alpha_d}{\Delta\theta} + \frac{\alpha_0+\alpha_d+\Delta\alpha_h}{\Delta\theta}\sqrt{1-\left(\frac{\alpha_0+\alpha_d+\Delta\alpha_h}{\Delta\theta}\right)^2} - \frac{\alpha_0-\alpha_d-\Delta\alpha_h}{\Delta\theta}\sqrt{1-\left(\frac{\alpha_0-\alpha_d-\Delta\alpha_h}{\Delta\theta}\right)^2} + \frac{\alpha_0+\alpha_d}{\Delta\theta}\sqrt{1-\left(\frac{\alpha_0+\alpha_d}{\Delta\theta}\right)^2} - \frac{\alpha_0-\alpha_d}{\Delta\theta}\sqrt{1-\left(\frac{\alpha_0-\alpha_d}{\Delta\theta}\right)^2} - 4a\frac{\omega c}{U}\left(2\frac{\alpha_d}{\Delta\theta}+\frac{\Delta\alpha_h}{\Delta\theta}\right)\frac{\Delta\alpha_h}{\Delta\theta}\right] - \frac{c_{m\alpha_1} - c_{m\alpha_2}}{\pi}$$

$$\times\left\{\left[4a^2\frac{\omega c}{U}\frac{\alpha_d}{\Delta\theta} - \frac{1}{(\omega c/U)}\frac{\Delta\alpha_h}{\Delta\theta}\right]\frac{\Delta\alpha_h}{\Delta\theta} - a\frac{\Delta\alpha_h}{\Delta\theta}\right.$$

$$\left.\times\left[\sqrt{1-\left(\frac{\alpha_0+\alpha_d+\Delta\alpha_h}{\Delta\theta}\right)^2} + \sqrt{1-\left(\frac{\alpha_0-\alpha_d-\Delta\alpha_h}{\Delta\theta}\right)^2}\right]\right\} \tag{13}$$

Subscripts *1* and *2* designate the derivative values for $\alpha < \alpha_d$ and $\alpha > \alpha_d$ respectively a is the total time lag parameter taking the place of $\Delta\tau_s$ Eq (7) Equation (13) shows that if aerodynamic hysteresis is present $\Delta\alpha_h \neq 0$ the measured damping derivative will become frequency sensitive Testing at two different frequencies [18] $f = 32$ and 45 Hz gave the same results within the data accuracy indicating that $\Delta\alpha_h = 0$ This was expected for the continuous flow characteristics at $M_\infty < M_c$ but there is always a good possibility that hysteresis effects accompany the discontinuous characteristics especially when they are caused by flow separation [12,24] With $\Delta\alpha_h = 0$ Eq (13) simplifies to

$$c_{m\dot{\theta}_s} = \frac{c_{m\dot{\theta}_1} + c_{m\dot{\theta}_2}}{2} + \frac{c_{m\dot{\theta}_1} - c_{m\dot{\theta}_2}}{\pi}\left[\arcsin\left(\frac{\alpha_d-\alpha_0}{\Delta\theta}\right) + \frac{\alpha_d-\alpha_0}{\Delta\theta}\sqrt{1-\left(\frac{\alpha_d-\alpha_0}{\Delta\theta}\right)^2}\right] - \frac{2a\Delta c_m}{\pi\alpha_d}\frac{\alpha_d}{\Delta\theta}\sqrt{1-\left(\frac{\alpha_d-\alpha_0}{\Delta\theta}\right)^2} \tag{14}$$

For the continuous flow characteristics at $M_\infty < M_c$ considered earlier Eqs (7 11) $\Delta\tau_s = 1\ 5$ However in this case of

sudden nose stall one has to add the transient effect of the "spilled' leading edge vortex [4] Thus,

$$a=\Delta\tau_s+\Delta\tau_v \tag{15}$$

It is shown in Ref 4 for a sharp leading edge that

$$\Delta\tau_v=2\ 5 \tag{16}$$

that is in the present case

$$a=4\ 0 \tag{17}$$

Figure 10 shows the nonlinear dynamic characteristics measured at $M=0\ 7$ for $\Delta h/h=0\ 55$ As indicated in the figure the discontinuity appeared at $\alpha_d=-2$ deg in the dynamic test [17] not $\alpha_d=-3$ deg, as in the static test [21] This difference is probably caused by the different test setups An end plated half model was used in the dynamic test [17 18] whereas the model extended from one sidewall to the other in the static test [21]

The topside flow remains totally separated, as is documented by the constant pressure (Figs 6 and 8) and is indicated by the flow sketches in Fig 10 At $\alpha_0<\alpha_d$ the underside is totally separated also and $c_{m\dot\theta}=0$ At $\alpha_0>\alpha_d$ the infinitesimal amplitude damping is probably well represented by $c_{m\dot\theta}$ for $\alpha_0=0$ shown in Fig 4b For $M_\infty=0\ 7$ the predicted value is $c_{m\dot\theta}=-1\ 95$ The measured discontinuity at $M_\infty=0\ 7$ is $\Delta c_m=-0\ 06$ (Fig 5) Thus one should use the following values in Eq (14):

$$c_{m\dot\theta_1}\approx 0,\qquad c_{m\dot\theta_2}\approx -1\ 95\qquad \Delta c_m\approx -0\ 06 \tag{18}$$

Using $\alpha_d=2$ deg Eqs (14) and (18) combine to give the predictions shown in Fig 11 The agreement between prediction and experiment is excellent, indicating that the simple analytical treatment has simulated the essential un steady flow characteristics Note that at $|\alpha_0-\alpha_d|>\Delta\theta$ the oscillation does not catch the discontinuity i e $c_{\dot m\dot\theta}=c_{m\dot\theta}$

The most adverse damping is obtained at $\alpha_0=\alpha_d$ for which case Eq (14) simply becomes

$$c_{\dot m\dot\theta_s}=\frac{c_{m\dot\theta_1}+c_{m\dot\theta_2}}{2}+\frac{2a\Delta c_m}{\pi\Delta\theta} \tag{19}$$

This gives the results shown in Fig 12 Again there is good agreement between prediction and experiment, both in dicating that positive damping, i e $c_{m\dot\theta}<0$ will not be measured until the amplitude exceeds 7 deg

Conclusions

The developed analytic relationships between unsteady and steady shock induced stall characteristics provide the capability to predict linear and nonlinear damping charac teristics for cross sections experiencing shock induced flow separation This has been demonstrated by successful prediction of the dynamic stall characteristics of rectangular cross sections representing different designs of the Space Shuttle cable trays

References

[1] McCroskey W J Recent Developments in Dynamic Stall *Proceedings University of Arizona/USAF OSR Symposium on Unsteady Aerodynamics* edited by R B Kinney Tucson Ariz March 1975, pp 1 33

[2] McCroskey W J The Phenomenon of Dynamic Stall NASA TM 81264 March 1981

[3] Ericsson L E and Reding, J P Dynamic Stall Analysis in Light of Recent Numerical and Experimental Results *Journal of Aircraft* Vol 13 April 1976 pp 248 255

[4] Ericsson L E and Reding J P Dynamic Stall at High Frequency and Large Amplitude *Journal of Aircraft* Vol 17 March 1980 pp 136 142

[5] McCroskey W J , McAllister K W Carr, L W Pucci S L , Lambert O and Indergrand R F Dynamic Stall on Advanced Airfoil Sections *Journal of the American Helicopter Society* Vol 26, July 1981 pp 40 50

[6] McCroskey W J , McAllister, K W Carr L W and Pucci S L An Experimental Study of Dynamic Stall on Advanced Airfoil Sections, Volume 1 Summary of the Experiment NASA TM 84245 July 1982

[7] Ericsson, L E and Reding J P Stall Flutter Analysis *Journal of Aircraft* Vol 10 Jan 1973 pp 5 13

[8] Ericsson L E and Reding J P , Unsteady Airfoil Stall Review and Extension *Journal of Aircraft* Vol 8 Aug 1971 pop 609 616

[9] Fung Y C *An Introduction to the Theory of Aeroelasticity* Dover Publ Inc N Y 1968 p 129

[10] von Kármán T and Sears W R Airfoil Theory for Non Uniform Motion *Journal of Aerospace Sciences* Vol 5 No 10 Aug 1938 pp 379 390

[11] Polhamus, E C 'Effect of Flow Incidence and Reynolds Number on Low Speed Aerodynamic Characteristics of Several Noncircular Cylinders with Applications to Directional Stability and Spinning NASA TR R 29 1959

[12] Ericsson, L E Unsteady Aerodynamics of Separating and Reattaching Flow on Bodies of Revolution, *Recent Research on Unsteady Boundary Layers Vol 1 UTAM Symposium* Laval University Quebec, May 1971 pp 481 512

[13] McCroskey W J Carr L W and McAllister K W Dynamic Stall Experiments on Oscillating Airfoils *AIAA Journal* Vol 14 Jan 1976 pp 57 63

[14] Ericsson L E , Dynamic Effects of Shock Induced Flow Separation *Journal of Aircraft* Vol 12, Feb 1975 pp 86 92; also Errata *Journal of Aircraft*, Vol 18 July 1981 p 608

[15] Lambourne N C Some Instabilities Airsing from the In teraction Between Shock Waves and Boundary Layers Aeronautical Research Council London C P 473 Feb 1958

[16] Ericsson L E and Reding J P , Aeroelastic Stability of Space Shuttle Protuberances *Journal of Spacecraft and Rockets* Vol 19 July Aug 1982 pp 307 313

[17] Orlik Rückemann K J and LaBerge J G Dynamic Wind Tunnel Tests of the Simulated Shuttle External Tank Cable Trays *Journal of Spacecraft and Rockets* Vol 20 Jan Feb 1983 pp 5 10

[18] LaBerge J G Dynamic Wind Tunnel Tests of the Shuttle External Tank Cable Trays at Subsonic Speeds LTR UA 55 NRC Canada Feb 1981

[19] Ericsson L E and Reding J P Aeroelastic Analysis of the Shace Shuttle External Tank Cable Trays Final Technical Report, Lockheed Missiles & Space Company Inc , Sunnyvale Calif LMSC D766543 April 1981

[20] Ericsson L E and Reding J P Subsonic Dynamic Stall in Pitching and Plunging Oscillations Including Large Ground In terference Effects ' AIAA Paper 83 0889 CP 24th Structures Structural Dynamics and Materials Conference Pt 2 May 1983 pp 266 276

[21] Michna, P J and Parker D R Test Results from the Pressure Test of a 12 Scale Model of the External Tank LO Cable Tray and GO Pressure Line and a 1575 Scale Model of the aft ET/SRB Cable Tray in the MSFC 14 Inch Trisonic Wind Tunnel Test No 661 Martin-Marietta Corporation Michoud Operations New Orleans La Rept MMC ET SE05 89 May 1980

[22] Revell J D and Cathaway R W Analysis of Transonic Airfoil Independent Research Data Based on Transonic Tests on Airfoils 1 to 4 Conducted at the ARA 8 ×18 2 D Transonic Wind Tunnel Lockheed California Co Burbank Calif LR23162 Feb 1970

[23] Lindsey W F and Landrum E J Compilation of In formation on the Transonic Attachment of Flows at the Leading Edge of Airfoils NACA TN 4204 Feb 1958

[24] Ericsson, L E Separated Flow Effects on the Static and Dynamic Stability of Blunt Nosed Cylinder Flare Bodies NASA CR 76919 Dec 1965